JGR Atmospheres

RESEARCH ARTICLE
10.1029/2019JD031526

Subtropical Cyclone Formation via Warm Seclusion Development: The Importance of Surface Fluxes

L. Quitián-Hernández[1], J. J. González-Alemán[2], D. Santos-Muñoz[3], S. Fernández-González[3], F. Valero[1,4], and M. L. Martín[4,5]

[1]Department of Astrophysics and Atmospheric Sciences, Faculty of Physics, Complutense University of Madrid, Madrid, Spain, [2]Environmental Sciences Institute, University of Castilla-La Mancha, Toledo, Spain, [3]State Meteorological Agency (AEMET), Madrid, Spain, [4]Interdisciplinary Mathematical Institute (IMI), Complutense University of Madrid, Madrid, Spain, [5]Department of Applied Mathematics, Faculty of Computer Engineering, University of Valladolid, Valladolid, Spain

Key Points:
- Observed warm seclusion process of a Shapiro-Keyser-like subtropical cyclone
- Surface turbulent heat fluxes played a key role during intensification of the cyclone
- No transition into a subtropical cyclone is found in absence of surface turbulent heat fluxes

Correspondence to:
L. Quitián-Hernández,
lquitian@ucm.es

Citation:
Quitián-Hernández, L., González-Alemán, J. J., Santos-Muñoz, D., Fernández-González, S., Valero, F., & Martín, M. L. (2020). Subtropical cyclone formation via warm seclusion development: The importance of surface fluxes. *Journal of Geophysical Research: Atmospheres*, *125*, e2019JD031526. https://doi.org/10.1029/2019JD031526

Received 1 OCT 2019
Accepted 4 MAR 2020
Accepted article online 12 MAR 2020

Author Contributions:
Conceptualization: J. J. González-Alemán, D. Santos-Muñoz, S. Fernández-González, F. Valero, M. L. Martín
Formal analysis: D. Santos-Muñoz, F. Valero, M. L. Martín
Investigation: J. J. González-Alemán
Methodology: L. Quitián-Hernández, M. L. Martín
Resources: J. J. González-Alemán, D. Santos-Muñoz
Software: L. Quitián-Hernández, S. Fernández-González
Supervision: D. Santos-Muñoz, M. L. Martín
Validation: L. Quitián-Hernández
(continued)

Abstract Subtropical cyclones (STCs) are characterized by a thermal hybrid structure with tropical and extratropical features. STCs are considered a numerical modeling challenge because of their rapid intensification. A fundamental part of their strength is derived from diabatic processes associated with convection and heat fluxes from the ocean. This study evaluates the importance of surface turbulent heat fluxes during the transition of an extratropical precursor into a STC. This cyclone evolved embedded within a strong meridional flow, having a Shapiro-Keyser structure and undergoing a warm seclusion process. To assess the importance of those heat fluxes, two Weather Research and Forecasting simulations were defined considering the presence and absence of those fluxes. Results of both simulations reveal a warm seclusion process, which weakened in absence of the heat fluxes. During the system genesis and in absence of heat fluxes, the wind and rainfall values were increased due to the remarkably intense area of frontogenesis to the northwest. Given these results and the lack of transition in the absence of heat fluxes, the frontal nature of the system was verified. Considering the heat fluxes, the obtained potential vorticity values diminished, reducing wind shear and intensifying convection in the system, which favored its transition into an STC. This study is groundbreaking in that no STC has been linked to a warm seclusion process in the Eastern North Atlantic. Additionally, simulated wind field shows an underestimation in comparison with Atmospheric Motion Vectors, used as observational data so as to give a weight to the wind analysis.

1. Introduction

For decades, the Eastern North Atlantic Ocean has had numerous extreme events, causing widespread loss and damage. Among them, intense subtropical cyclones (STCs) like Tropical Storm Delta (2005) and Hurricane Vince (2005) were identified as STCs in their early stages (González-Alemán et al., 2015). More recent examples Hurricane Alex (2010), Ophelia (2017), and Leslie (2018) acquired a subtropical structure at some point in their lifecycles. Moreover, the STC hybrid characteristics have also been observed in other locations, like the South Atlantic Ocean, where STC Anita even acquired potential characteristics to almost transition to Hurricane (Dias Pinto et al., 2013). STC study remains a challenge for meteorological services worldwide because of the dominant role of convective processes that induce a characteristic hybrid thermal structure, rapid intensification, and great intensity. These characteristics are similar in some cases to hurricanes or tropical storms. The number of studies focusing on STCs and their particular characteristics has clearly increased, which has even led to STC climatologies (Cavicchia et al., 2019; Evans & Guishard, 2009; Evans & Braun, 2012; González-Alemán et al., 2015; González-Alemán et al., 2018; Guishard et al., 2007; Guishard et al., 2009).

From a dynamical and thermodynamic points of view, Quitián-Hernández et al. (2016) analyzed a STC that occurred between 18 and 22 October 2014 near the Canary Islands. During the October 2014 STC formation, there was a remarkable meridional atmospheric circulation over the Eastern North Atlantic. This synoptic situation in conjunction with a low-level baroclinic zone favored the formation and later isolation of this cyclone. Moreover, as occurs during the development of an EC, owing to strong latent heat release, there is rapid deepening at the cyclone center (Davolio et al., 2009; Kuo et al., 1991; Miller & Katsaros, 1992; Reed et al., 1988). This triggers an intense convective response as the result of strong heat and moisture

Writing - original draft: L. Quitián-Hernández
Writing – review & editing: J. J. González-Alemán, D. Santos-Muñoz, S. Fernández-González, F. Valero, M. L. Martín

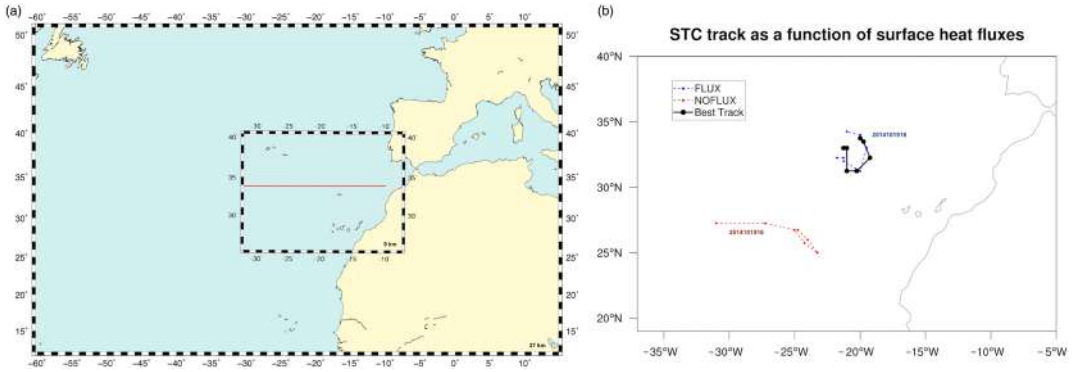

Figure 1. (a) WRF model domains used. Domain 2 is shown at the beginning of simulation. Red line shows location of E-W vertical cross section used. (b) STC track as a function of surface heat fluxes during the pre-STC period.

advection, causing strong winds and precipitation. Frequent flooding, flight cancelations, electrical storms, and fires were only some of the impacts of the STC on Tenerife Island. Rapid deepening, very characteristic of such systems, requires optimal numerical models to improve their prediction. Quitián-Hernández et al. (2018) conducted a sensitivity analysis of diverse parameterization schemes using the Weather Research and Forecasting (WRF) model for the genesis and intensification of the aforementioned STC.

Furthermore, these extreme cyclones can transition from one to another, making us more aware of how potentially dangerous can these atmospheric systems be. Some authors have stated that sheared baroclinic extratropical cyclones (ECs) evolve into warm-core tropical cyclones (TCs), involving a remarkable tropical transition (TT) (Hulme & Martin, 2009a, 2009b). This also occurs with STCs. However, more studies of STC formation and development are necessary to better understand the mechanism of intensification of this type of cyclone and improve its prediction. Moreover, in several TT studies (Cordeira & Bosart, 2010; Cordeira & Bosart, 2011; Hulme & Martin, 2009a, 2009b), it has been observed that extratropical precursors are required for the transition, which is characterized by a Shapiro-Keyser-like structure (Shapiro & Keyser, 1990), that is, a bent-back warm/occluded front that undergoes a warm seclusion process (Bentley & Metz, 2016; Davis & Bosart, 2004). The warm seclusion process has been observed in studies of transitions into tropical systems (Bentley & Metz, 2016; Mazza et al., 2017), or even of "Medicanes" over the Mediterranean Sea (Mazza et al., 2017; Miglietta & Rotunno, 2019). Furthermore, it has been found a relationship between a warm seclusion process and STC development over the eastern Australian seaboard (Browning & Goodwin, 2013; Mills et al., 2010). However, there are no studies that correlate a warm seclusion process with STCs in the North Atlantic Ocean.

According to Schultz et al. (1998), there are two conceptual models (Norwegian and Shapiro-Keyser) that attempt to describe the frontal structure and evolution of midlatitude cyclones. According to that work, those cyclones evolve from a confluent, low-amplitude zonal atmospheric circulation developing robust, zonally elongated frontal areas and resembling a Shapiro-Keyser structure. However, in this paper we show that the October 2014 STC was formed from a meridional flow that acquired the same Shapiro-Keyser configuration. Consequently, this presents a novel and interesting case study to analyze. Thus, with reference the sensitivity study of Quitián-Hernández et al. (2018) and the present results, we analyzed different fields to ascertain if the examined STC underwent a warm seclusion process. Regarding this TT paradigm, a strong near-surface easterly flow to the north of the system plays a critical role in TC development (Galarneau et al., 2015). This results in an increment of oceanic latent heat flux transport, facilitating the generation of deep moist convection. Several authors have tested the effects of latent heat fluxes on cyclone development (Gozzo et al., 2017; Gozzo & da Rocha, 2013; Kuo et al., 1991; Miglietta & Rotunno, 2019). However, few studies have focused on the effects of surface fluxes on the development of a Shapiro-Keyser-like STC. Thus, we explored the key role of surface turbulent heat fluxes during the development and intensification of the October 2014 STC by evaluating numerical experiments with the presence (CNTL run) or absence (NOFLUX run) of surface turbulent heat fluxes.

We briefly present the data sets, domain specification, and numerical model setup in section 2. Section 3 gives a synoptic description of the case study and methodology. Section 4 includes a discussion of the results and

Table 1
Sensitivity Experiments Configuration

	Microphysics	Longwave radiation	Shortwave radiation	Cumulus	Experiment
WSM5-Dudhia-KF	WSM5	RRTM	Dudhia	Kain-Fritsch	411
WSM5-Dudhia-Tiedtke	WSM5	RRTM	Dudhia	Tiedtke	416
WSM5-Dudhia-OldKF	WSM5	RRTM	Dudhia	Old Kain-Fritsch	419
WSM5-RRTMG-KF	WSM5	RRTMG	RRTMG	Kain-Fritsch	441
WSM5-RRTMG-Tiedtke	WSM5	RRTMG	RRTMG	Tiedtke	446
WSM5-RRTMG-OldKF	WSM5	RRTMG	RRTMG	Old Kain-Fritsch	449
WSM6-Dudhia-KF	WSM6	RRTM	Dudhia	Kain-Fritsch	611
WSM6-Dudhia-Tiedtke	WSM6	RRTM	Dudhia	Tiedtke	616
WSM6-Dudhia-OldKF	WSM6	RRTM	Dudhia	Old Kain-Fritsch	619
WSM6-RRTMG-KF	WSM6	RRTMG	RRTMG	Kain-Fritsch	641
WSM6-RRTMG-Tiedtke	WSM6	RRTMG	RRTMG	Tiedtke	646
WSM6-RRTMG-OldKF	WSM6	RRTMG	RRTMG	Old Kain-Fritsch	649
Thompson-Dudhia-KF	Thompson	RRTM	Dudhia	Kain-Fritsch	811
Thompson-Dudhia-Tiedtke	Thompson	RRTM	Dudhia	Tiedtke	816
Thompson-Dudhia-OldKF	Thompson	RRTM	Dudhia	Old Kain-Fritsch	819
Thompson-RRTMG-KF	Thompson	RRTMG	RRTMG	Kain-Fritsch	841
Thompson-RRTMG-Tiedtke	Thompson	RRTMG	RRTMG	Tiedtke	846
Thompson-RRTMG-OldKF	Thompson	RRTMG	RRTMG	Old Kain-Fritsch	849

consequent evidence in the case study of development from a warm seclusion process, analyzing the major role of surface turbulent heat fluxes during that development. Finally, the main conclusions are summarized in section 4.

2. Domain Specification and WRF Model Setup

The analyzed variables were numerically simulated using the three-dimensional, nonhydrostatic Advanced WRF model Version 3.8 (Powers et al., 2017; Skamarock & Klemp, 2008). In our study, the model was configured with two nested domains of 27 and 9 km. Domain 1 (D01) had 217 × 150 grid points in the west-east and south-north directions, respectively, whereas Domain 2 (D02) had 237 × 180 grid points in the same directions. In order to maintain consistency with respect to the previous work of Quitián-Hernández et al. (2018), on which this work is based, the same WRF configuration is here used and described below. The initial/boundary conditions used for the STC simulation were taken from the National Centers for Environmental Prediction Global Forecast System analysis with 1° horizontal resolution at each 6 hr. The high-resolution inner domain was moved with the cyclone to accurately analyze its evolution. Both domains used 36 sigma levels uneven spaced, with more levels in the lower atmosphere for better representation of convection and boundary layer processes. Model domain configurations are shown in Figure 1.

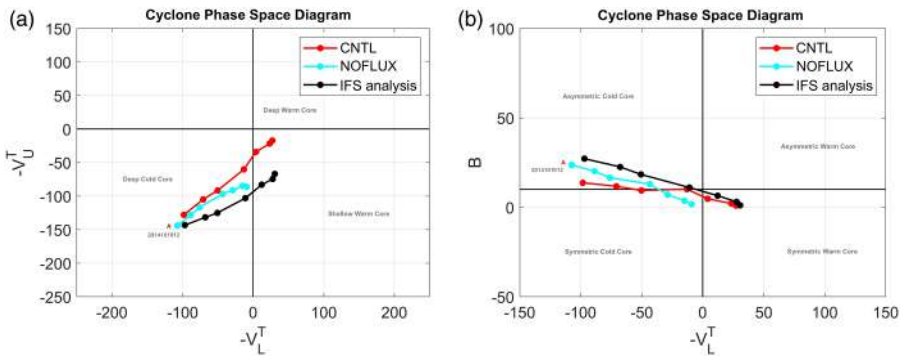

Figure 2. IFS analysis plotted in CPS for Experiment 616: (a) V_T^L versus V_T^U and (b) V_T^L versus B (m). Start of cyclone lifecycle (18 at 1200 UTC) is labeled by an A, and markers are placed every 6 hr.

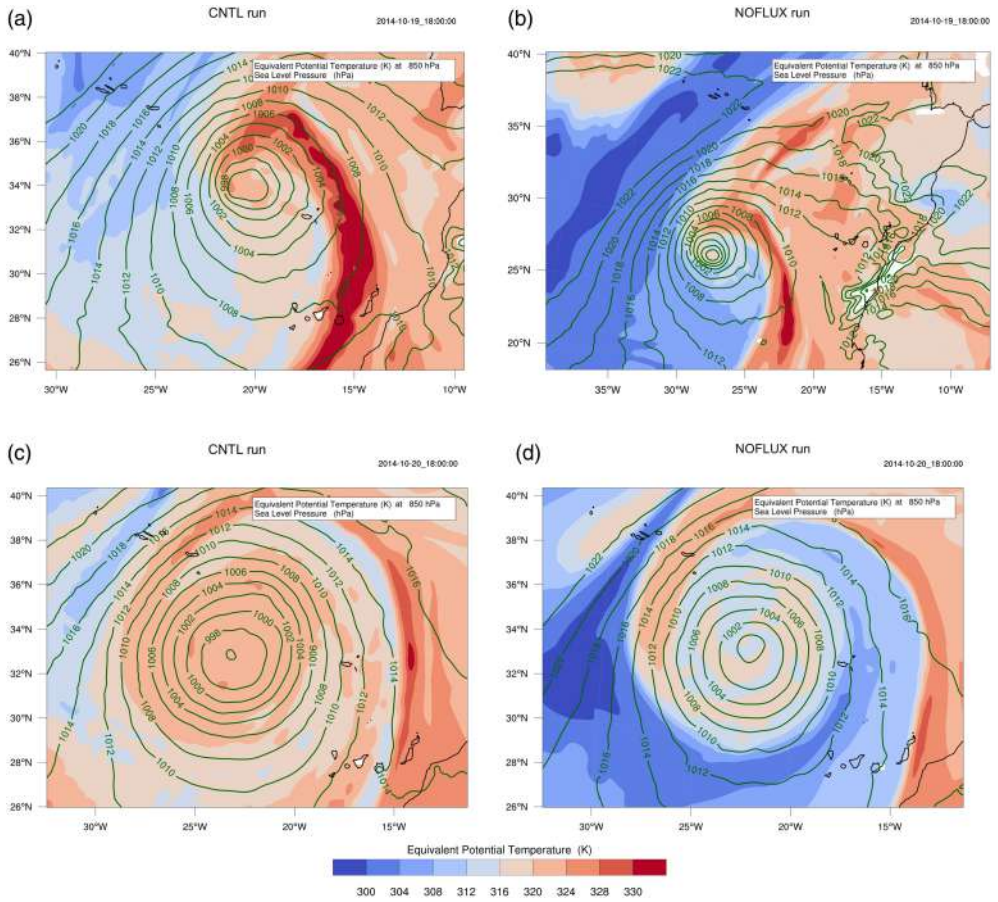

Figure 3. Simulated equivalent potential temperature (shaded, K) and sea level pressure (brown contours, hPa) on (a) 19; (c) 20 October 2014 at 1800 UTC (left) with the presence of surface turbulent heat fluxes, and on (b) 19; (d) 20 October 2014 at 1800 UTC (right) in absence of those fluxes.

Based on various scheme combinations that were tested in our previous study (Quitián-Hernández et al., 2018; tested combinations can be found in Table 1), we used the WSM6 scheme as the microphysical parameterization, Dudhia and RRTM schemes as the shortwave and longwave radiation parameterizations, respectively, and the Tiedtke as the cumulus parameterization scheme. Readers may refer to Quitián-Hernández et al. (2018) for detailed comparison of different combinations.

Note. Each experiment number corresponds to a WRF parameterization scheme.

Finally, to cover the entire STC life cycle, the period of integration extended from 1200 UTC on 18 October 2014 through 0000 UTC on 23 October 2014 (more information about the experimental design is in Quitián-Hernández et al., 2018). To analyze the impact of surface turbulent heat fluxes during STC evolution, an additional STC simulation was executed in the same way as the first, but the presence of heat fluxes was eliminated.

3. Results and Discussion

3.1. CPS Framework

Following the use of cyclone phase space (CPS; Hart, 2003) diagrams in Quitián-Hernández et al. (2018), we did a similar analysis to evaluate the importance of surface turbulent heat fluxes during STC genesis. These diagrams are based on several variables that provide information about different aspects of the cyclone. We investigated lower (900–600 hPa) and upper (600–300 hPa) tropospheric thermal winds ($-V_T$) (using 24-hr running means) to characterize the vertical thermal structure of the cyclone, that is, its cold or warm core. Moreover, we also analyzed the cyclone thermal symmetry (B), that is, the frontal nature strength, by means

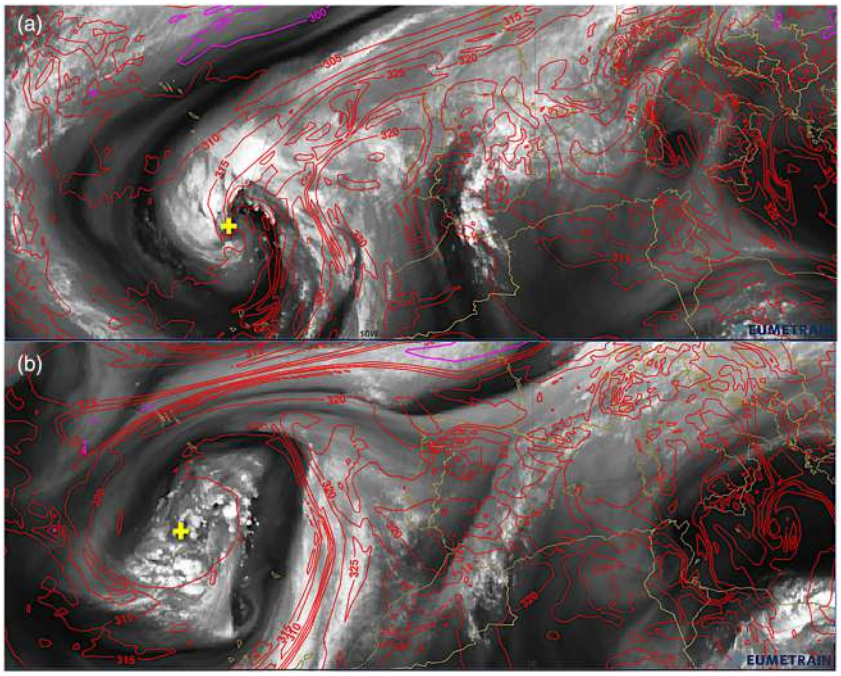

Figure 4. ECMW equivalent potential temperature (red contours) at 850 hPa over the MSG 6.2WV channel on (a) 19 and (b) 20 October 2014 at 1800 UTC. Pink contour corresponds to $\theta_e = 300$ K. Cyclone center is identified by yellow cross (available online at http://eumetrain.org/eport/archive_atlantic.html?width=1440&height=900).

of the storm motion-relative 900- to 600-hPa thickness gradient across the cyclone. The ($-V_T^L$; $-V_T^U$) CPS diagram for Experiment 616 that considered the presence of surface heat flux (red line of Figure 2) shows a deep cold core during the STC early stage, that is, 19 October and the early hours of 20 October. Therefore, during this stage the cyclone was categorized as a purely extratropical low. Afterward, the system developed a shallow warm core, typical of STCs. According to Quitián-Hernández et al. (2018), this transition from EC to STC was consistent with the analysis ($-V_T^L$; $-V_T^U$) CPS diagram obtained from the ECMWF Integrated Forecast System analysis database (black line of Figure 2). The CNTL run showed good agreement with the results that were calculated by using the ECMWF Integrated Forecast System analysis data (ECMWF, 2014; Figure 2), suggesting the results of our simulation are robust. These results confirm the skill of the WRF to simulate the system, while, when surface heat flux effects were eliminated, the EC did not transition to a STC (Figure 2, NOFLUX). Throughout its genesis and maturity, the cyclone was consistently an EC in the NOFLUX run. On the other hand, the ($-V_T^L$; B) CPS diagram for CNTL experiment (red line of Figure 2b) reveals that the system was developed in a weak baroclinic environment during the STC early stage. Around the early hours of 20 October, the cyclone moved to a more baroclinic one and attained a symmetric thermal structure by 1200 UTC, showing typical subtropical features. Nevertheless, when the surface heat fluxes were eliminated, the cyclone did not acquire a symmetric warm core (cyan line of Figure 2b, NOFLUX). Therefore, in the NOFLUX run, the system maintained a purely extratropical nature. Next, we determined if other atmospheric fields were modified as a function of these fluxes.

3.2. Warm Seclusion and Upstream Convection Propagation

During the days prior to acquiring subtropical characteristics (1800 UTC on 19 October), a well-defined frontal structure was found corresponding to an extratropical stage (Figure 3a). Once the cyclone attained a subtropical character (1800 UTC on October 20), there was a remarkable increase in the θ_e values around the cyclone center (Figure 3c). Analyzing Figure 4, the θ_e, obtained from the ECMWF model and shown by red contours on the Meteosat Second Generation (MSG) 6.2-μm water vapor channel for the same days (19 and 20 October at 1800 UTC), reveals a warm seclusion that formed around the cyclone center by the latter day (Figure 4b). These findings and the evolution of satellite images confirm that the warm seclusion process was well simulated by WRF (Figures 3a and 3c).

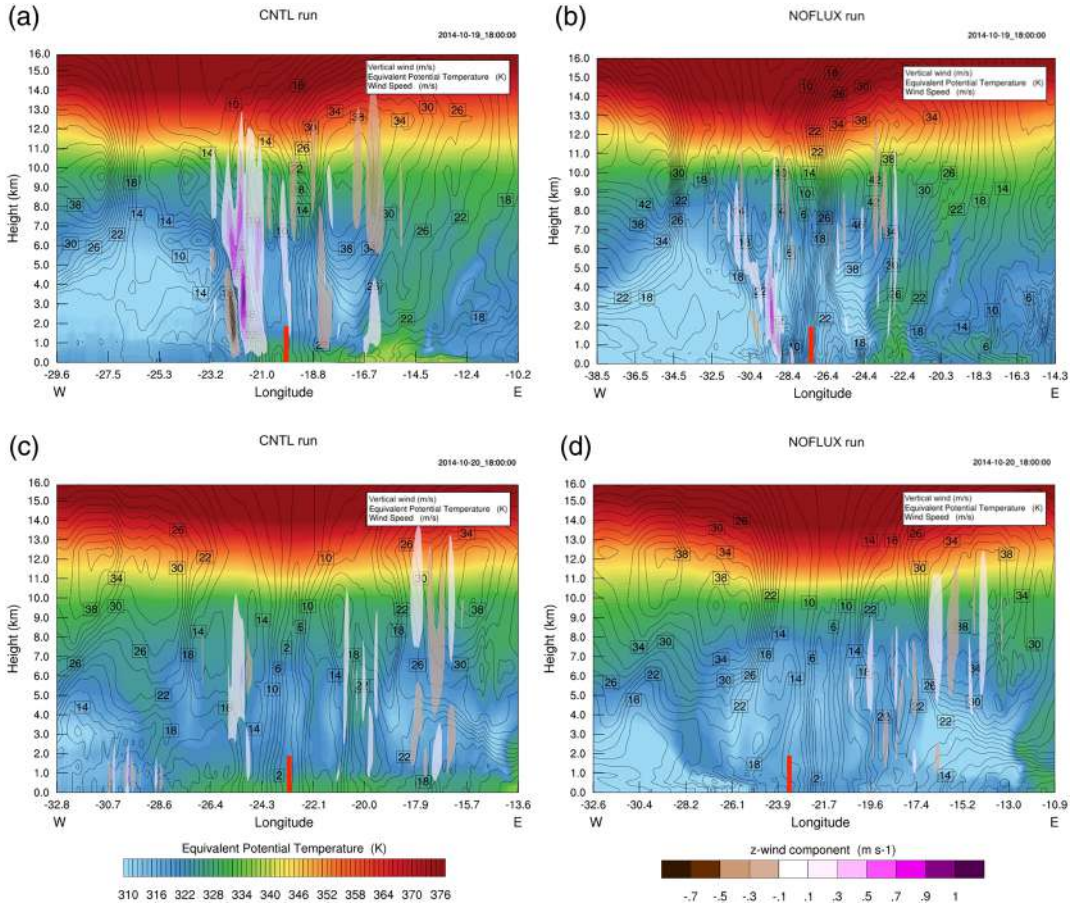

Figure 5. Simulated wind speed (contours, m/s), equivalent potential temperature (shaded in rainbow colors, K) and vertical wind (shaded in brown-to-purple colors, m/s) in west-east vertical cross section for (a) 19; (c) 20 October 2014 at 1800 UTC (left) with the presence of surface turbulent heat fluxes, and on (b) 19; (d) 20 October 2014 at 1800 UTC (right) in absence of those fluxes. System center is indicated by red vertical line.

The October 2014 STC evolution is consistent with the results of Davis and Bosart (2003, 2004) and Hulme and Martin (2009a), wherein a cold-core cyclone developed from the incursion of an upper-level trough in a low-level baroclinic zone. According to these authors, this constitutes a necessary condition for a TT. However, in the current case study and considering the presence of heat fluxes, the extratropical precursor transferred into a STC (Figure 2, CNTL). Furthermore, this cold-core EC, needed for the transition to take place, developed a bent-back warm front on its northern and western sides (Cordeira & Bosart, 2010; Cordeira & Bosart, 2011; Hulme & Martin, 2009b; Shapiro & Keyser, 1990). Consequently, a warm seclusion could occur that favored the transition, in this case, into a STC.

The NOFLUX simulation (Figures 3b and 3d) indicates that the cyclone maintained a warm seclusion structure, except θ_e is much weaker than in the CNTL run (Figures 3a and 3c). Furthermore, no transition to a STC was reproduced in the NOFLUX run (Figure 2, NOFLUX), corroborating the key role of those fluxes during system intensification. Another difference is a new location of the cyclone center. Upon canceling the turbulent surface heat fluxes, there was a remarkable southern displacement on the first day (19 October at 1800 UTC) (Figures 1b and 3b), that is, when according to the CPS diagram the system was purely an EC. This displacement can also be appreciated in Figure 3 by comparing the position of the cyclone vortex (during the pre-STC stage) with the location of the Canary Islands. However, a similar location was produced by both simulations for the second day (Figures 3c and 3d). According to several previous studies (Yanase et al., 2004; Miglietta & Rotunno, 2019), the suppression of a specific physical mechanism in a numerical simulation may cause major changes, not only in system evolution but also in the environment in which it developed. In fact, this could be one of the reasons why, in the early stages of the system (19

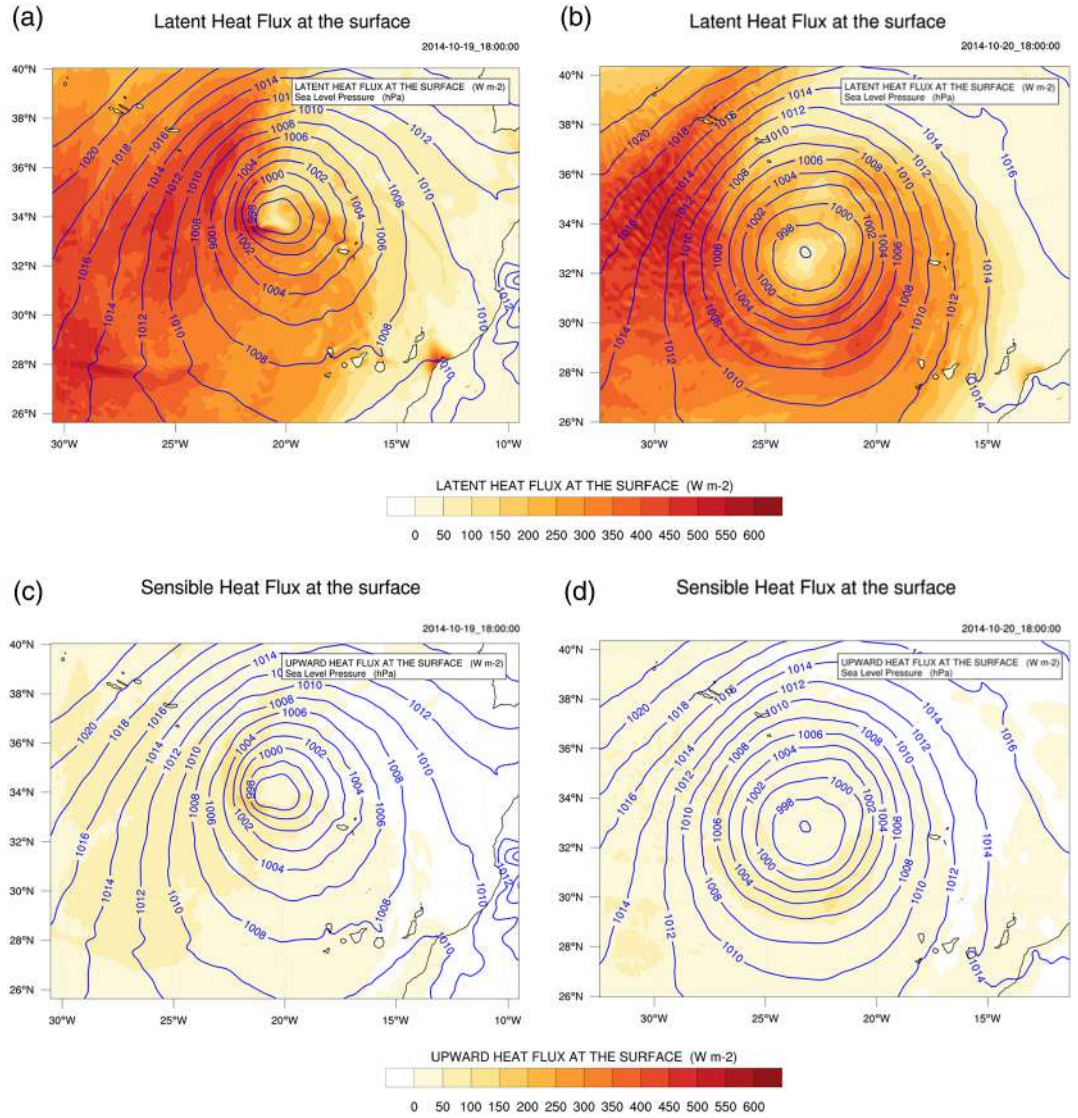

Figure 6. Simulated latent (top) and sensible (bottom) heat flux (shaded, W/m^2) plus sea level pressure (blue contours, hPa) on (a, c) 19 and (b, d) 20 October 2014 at 1800 UTC.

October at 1800 UTC), the lack of surface turbulent heat fluxes could cause differences in the STC genesis and displacement of the vortex (Figures 3b and 3d). However, once the system matured, the dynamical processes were relaxed and the displacement was much less remarkable.

In order to demonstrate the prominent role played by the intense heat and moisture from the ocean in low-level convection, the vertical velocity together with the horizontal wind speed (SPD) and θ_e fields were analyzed along the W-E vertical cross section shown in Figure 1. There are major differences in temperature between upper (warmer) and lower (colder) levels. However, during the pre-STC period (Figure 5a), a higher surface θ_e was reproduced in the eastern part of the cyclone, an area of heat and moisture advection (greenish tones at the surface in Figure 5a). In association, intense vertical currents are evident, promoting the upstream propagation of convection during the pre-STC phase (Figure 5a). This upstream propagation is also confirmed by the strong gradients of horizontal wind speed in the eastern part of the cyclone, coinciding with that intense vertical currents (Figure 5a) during the pre-STC period. Once the system acquired a subtropical structure (Figure 5c), the θ_e and vertical velocity values decreased considerably, facilitating the stabilization of convection.

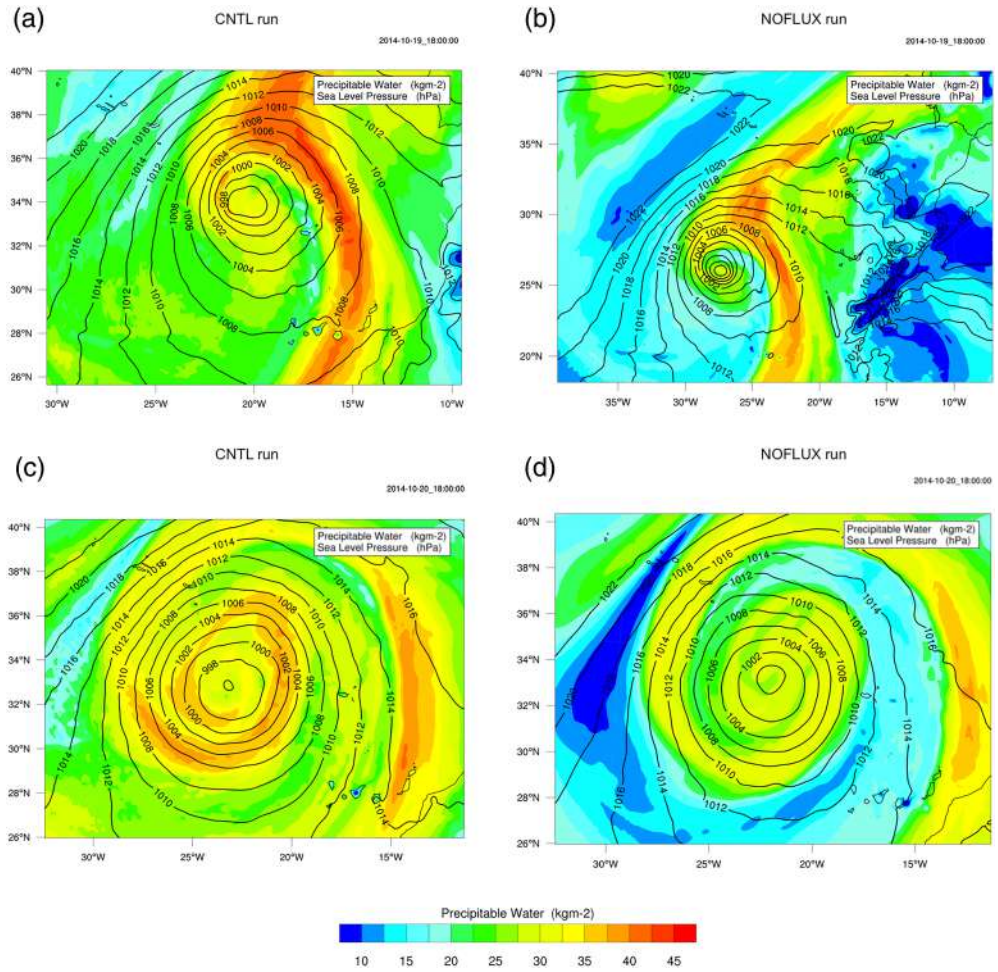

Figure 7. Same as Figure 3 except for precipitable water (shaded, kg/m^2).

From the results in absence of surface turbulent heat fluxes, there was a general reduction of the vertical velocity for both days (October 19 and 20 at 18 UTC). However, during the first day and compared to the second analyzed day (Figure 5b), relatively strong vertical currents were simulated. These results corroborate the key role of the surface turbulent heat fluxes during the upstream propagation of convection and system intensification. Miglietta and Rotunno (2019) stated in their study of Medicanes that in the NOFLUX run, colder values of θ_e were obtained at lower levels, maintaining active baroclinic instability in the early stages of those cyclones. When the turbulent surface fluxes were eliminated, we also found a notable reduction in θ_e at lower levels for our system (Figures 5b and 5d) and during the first day (Figure 5b), which corresponds to the EC stage.

Figure 6 shows the latent and sensible heat fluxes during the pre-STC (panels a and c, respectively) and pure STC stages (panels b and d). Large latent and sensible heat values were simulated around the western part of the cyclone during the pre-STC period (panels a and c). This increase in surface turbulent heat fluxes enhanced the propagation of deep convection in that area, strengthening the cyclone. Once the cyclone attained a hybrid STC structure, surface turbulent heat fluxes became scattered all around the cyclone center. Stronger latent heat fluxes (Figure 6b) and greater sensible heat fluxes (Figure 6d) were maintained around the northwest sector of the system, even extending to the southeast sector. Although the warm seclusion process was also evident even in the NOFLUX run with relative lower θe (Figure 3), it was much weaker than that in CNTL run, indicating the strong relationship between the surface heat fluxes and the intensity of the warm seclusion process (i.e., the Shapiro-Keyser cyclone development).

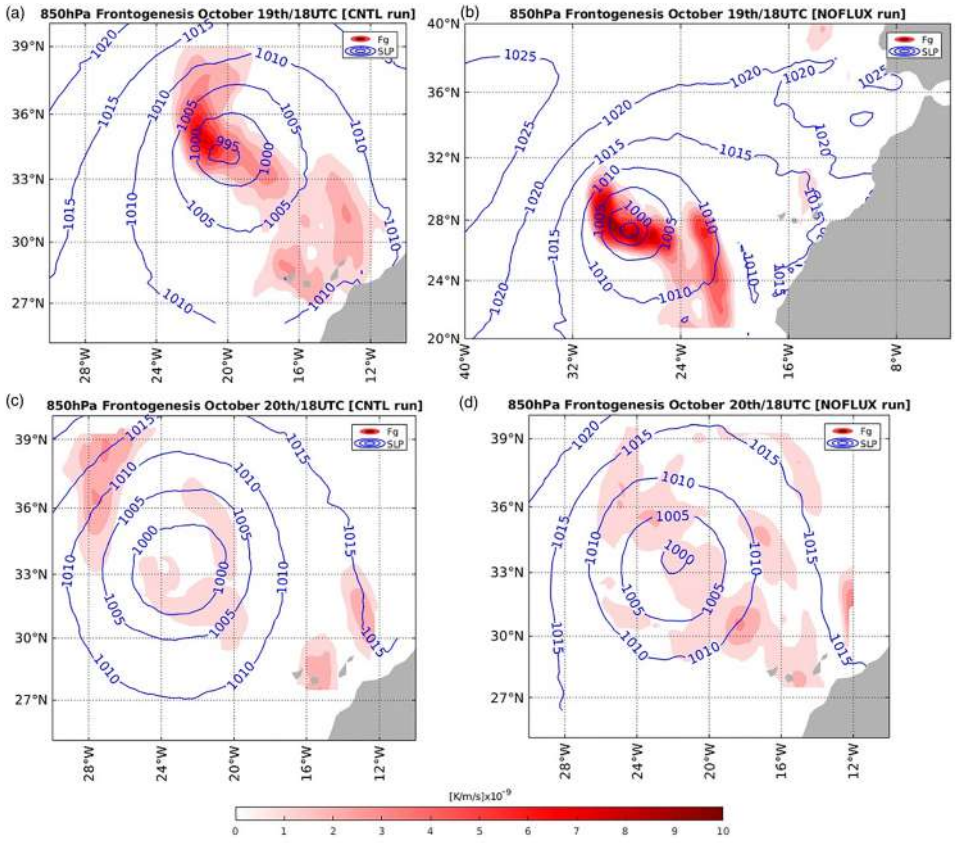

Figure 8. Same as Figure 3 except for 850-hPa frontogenesis (shaded, $K \cdot m^{-1} \cdot s^{-2} \cdot 10^{9}$) and sea level pressure (blue contours, hPa).

In addition to the weakening of the warm seclusion process of the October 2014 STC, there was a reduction of the precipitable water when the surface turbulent heat fluxes were disregarded (Figures 7b and 7d), highlighting again the importance of surface turbulent heat fluxes in system intensification and upstream convection propagation. Furthermore, we highlight the displacement of the cyclone center during the pre-STC stage (Figure 7b), with the cyclone essentially in the same location in both simulations for the pure-STC stage (Figures 7c and 7d).

The important relationship between the surface heat fluxes and the intensity of the Shapiro-Keyser development is directly related to the dominant role played by the convective processes. Those processes, mainly located around the cyclone northwestern area, lead to the intensification of the cyclone. Once the warm seclusion process characterized a Shapiro-Keyser-like structure during the genesis of the STC, we turned to the relationship between that process and upstream deep convection around the northwestern flank of the cyclone. A precursor favoring a TT is an upper-tropospheric trough that moves equatorward into a low-level baroclinic zone (Hulme & Martin, 2009a, 2009b). This environment is characterized by intense vertical wind shear that impedes the formation of tropical cyclones from tropical waves and deforms the baroclinic zone into a frontal wave (Martin, 2006). However, because of latent heat release in the atmospheric column, there is a redistribution of potential vorticity (PV), weakening the vertical wind shear field (Bentley & Metz, 2016; Posselt & Martin, 2004). In addition, air-sea interaction processes intensify the low-level cyclone (Emanuel, 1986). All the results associated to the relationship between the Shapiro-Keyser development and upstream deep convection will be displayed and analyzed hereunder.

According to Hulme and Martin (2009a, 2009b) and Cordeira and Bosart (2010, 2011), in order to have a TT, a precursor cold-core structure should develop with a Shapiro-Keyser-like structure. However, there is no evidence that this process always leads to Shapiro-Keyser-like cyclone development. For the studied STC, the extratropical precursor evolved similarly to the one described by Shapiro and Keyser (1990), in which

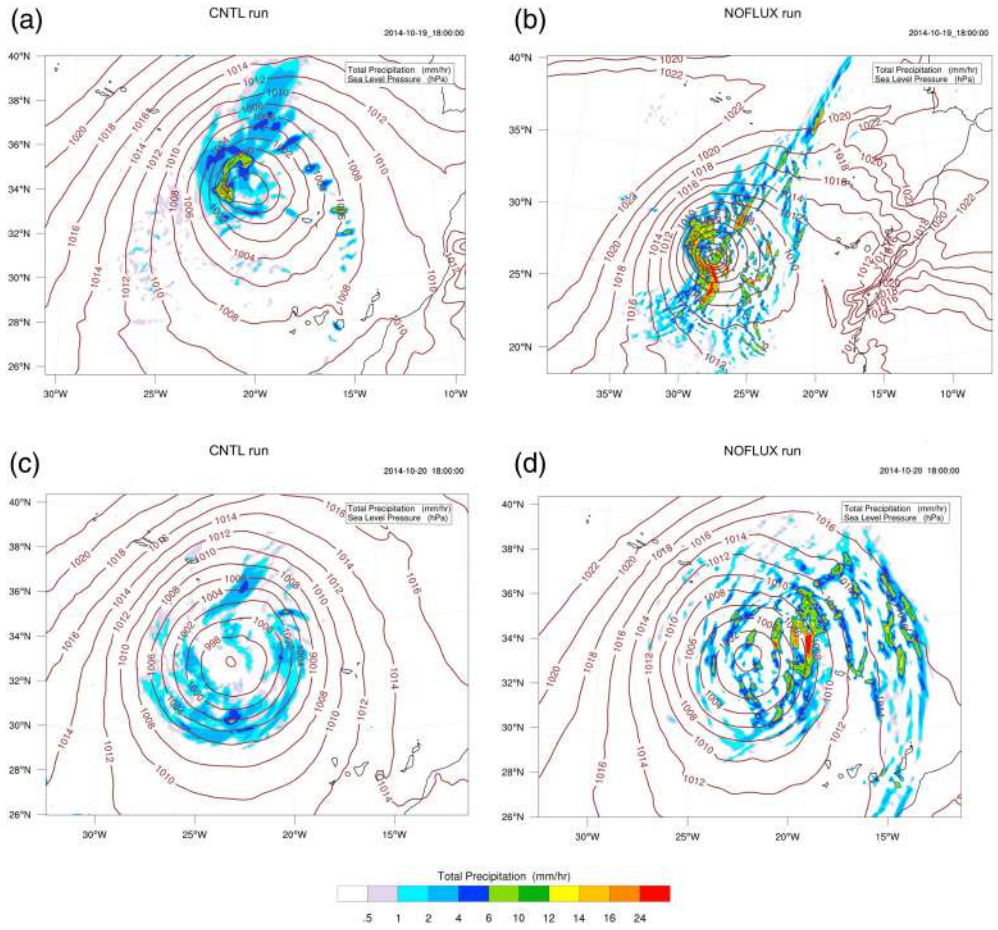

Figure 9. Same as Figure 3 except for precipitation (shaded, mm/hr) and sea level pressure (brown contours, hPa).

the warm/occluded front bent back into cool air to the west and northwest of the cyclone minimum pressure. Positive frontogenesis indicates an enhance of the horizontal temperature gradients with time. Consequently, the strengthening of an existing front will take place. Hulme and Martin (2009a, 2009b) identified an area of frontogenesis that intensified with time, promoting precipitation and lower tropospheric PV production via latent heat release. As a result, the likelihood of convective systems developing in that area is potentially increased. In fact, during the pre-STC period (Figure 8a), there were larger values of frontogenesis around the northwestern side of the cyclone. According to the results of Hulme and Martin (2009), in conjunction with this localized intense frontogenesis, precipitation develops there. This phenomenon is portrayed in Figure 9a. However, once the cyclone acquired subtropical characteristics, the frontogenesis (Figure 8c) and precipitation values (Figure 9c) were considerably reduced. Combined with the intense heat fluxes around the cyclone northwestern flank on the same day (Figure 6), particularly those of latent heat (Figure 6a), the above results effectively reveal the essential role of the surface heat fluxes during STC intensification.

Considering the absence of surface turbulent heat fluxes (Figures 8b and 8d), the frontogenesis showed a noticeable boost on both analyzed days (nineteenth and twentieth at 1800 UTC). In addition, on the EC stage (Figure 8b), a frontogenesis maximum persisted around the northwestern side of the cyclone, even extending to its center. Note the displacement of that center toward the south at 1800 UTC on 19 October (Figure 8b), in contrast to the similar location produced by both simulations for the pure STC (Figures 8c and 8d). With the absence of surface turbulent heat fluxes in the EC period (Figure 9b), there was a remarkable increase in precipitation around the northwestern flank of the cyclone and warm/occluded front structure. A deviation of the cyclone center is again found on the EC stage (nineteenth at 1800 UTC). On 20

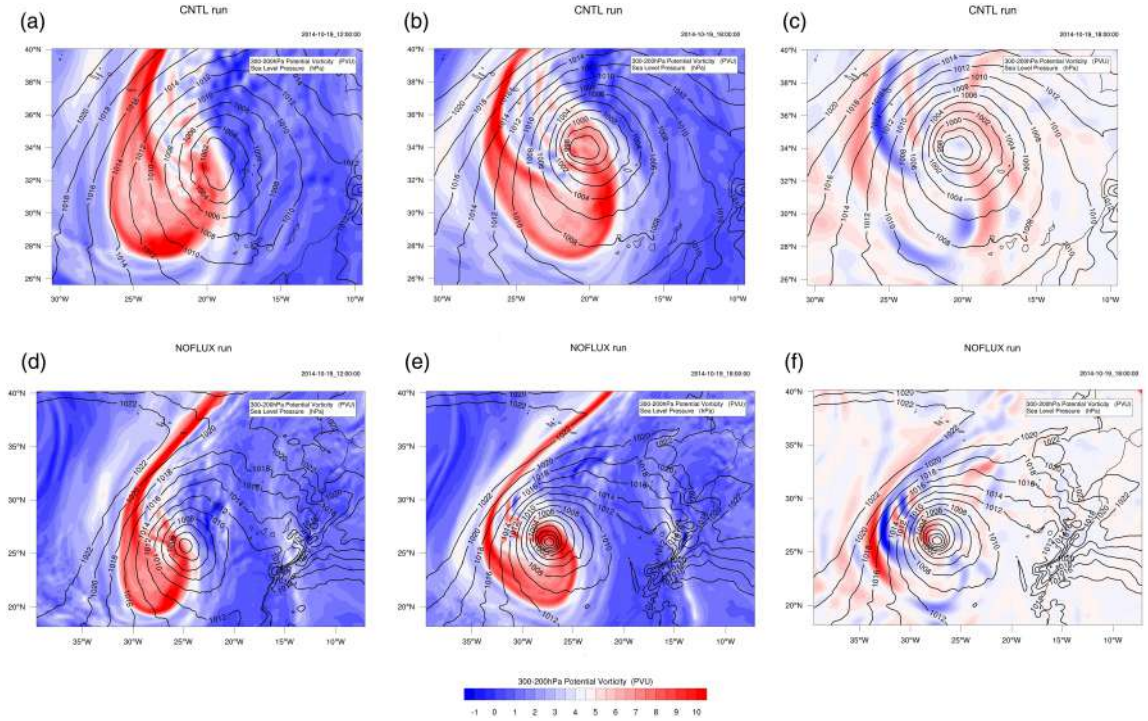

Figure 10. Simulated sea level pressure (black contourns, hPa) and (a, b, d, and e) 300- to 200-hPa potential vorticity (shaded, PVU); (c, f) 300- to 200-hPa potential vorticity tendency (shaded, PVU) on 19 October 2014 at 1800 UTC. Top panels show the variables with the presence of surface fluxes and bottom panels in absence of those fluxes.

October, however, during which a frontal character persisted in the NOFLUX run, precipitation increased on the northeast-east side of the system (Figure 9d).

Considering the surface turbulent heat fluxes, defined as CNTL run, in association with latent heat release, there was a vertical redistribution of PV over the cyclone center (top panels of Figures 10 and 11), consisting of previous studies (Bentley & Metz, 2016; Davis & Bosart, 2004; Hulme & Martin, 2009). Consequently, there was a noticeable decrease in PV values from the pre-STC stage (Figures 10a and 10b) to the fully formed STC (Figures 11a and 11b). In contrast, in the NOFLUX run, there was a general increase in PV values (Figures 10d and 10e and 11d and 11e) and PV tendency (Figures 10f and 11f) on both days. This confirms that the atmospheric dynamics alone can contribute to the warm seclusion process, but not a transition from EC to STC—the surface turbulent heat fluxes are crucial for that.

Overall, a remarkable latent heat release to the northwest caused the redistribution of PV during STC evolution (top panels of Figures 10 and 11). Regarding the results with the presence of surface turbulent heat fluxes, larger PV values were obtained for the pre-STC period (Figures 10a and 10b). There was also a weakening of the wind shear field (Figures 12a and 12c), due to the convective intensification, promoted by those heat fluxes, that triggered the rainfall in the northwestern area. Also in that area, intense frontogenesis was simulated (Figure 8a), promoting intense precipitation (Figure 9a). Moreover, in order to verify the crucial role played by the latent heat release during the intensification of the system, an extra simulation was assessed canceling the latent heat release and maintaining the surface turbulent heat fluxes. Analyzing the results (not shown), it can be concluded that the deactivation of the latent heat release causes an enhancement of the wind shear, which limits the system intensification and preserve its extratropical nature.

In the NOFLUX run, PV values were generally larger (bottom panels of Figures 10 and 11) than those obtained in the CNTL run (top panels of those figures). Likewise, larger values were obtained for the EC period (Figures 10d and 10e). The boost in the PV field in the NOFLUX run could be related to a lower availability of water vapor in absence of turbulent surface heat fluxes. Therefore, less amount of PV in upper levels could be destroyed in the cyclogenesis process when that such water vapor condenses and latent

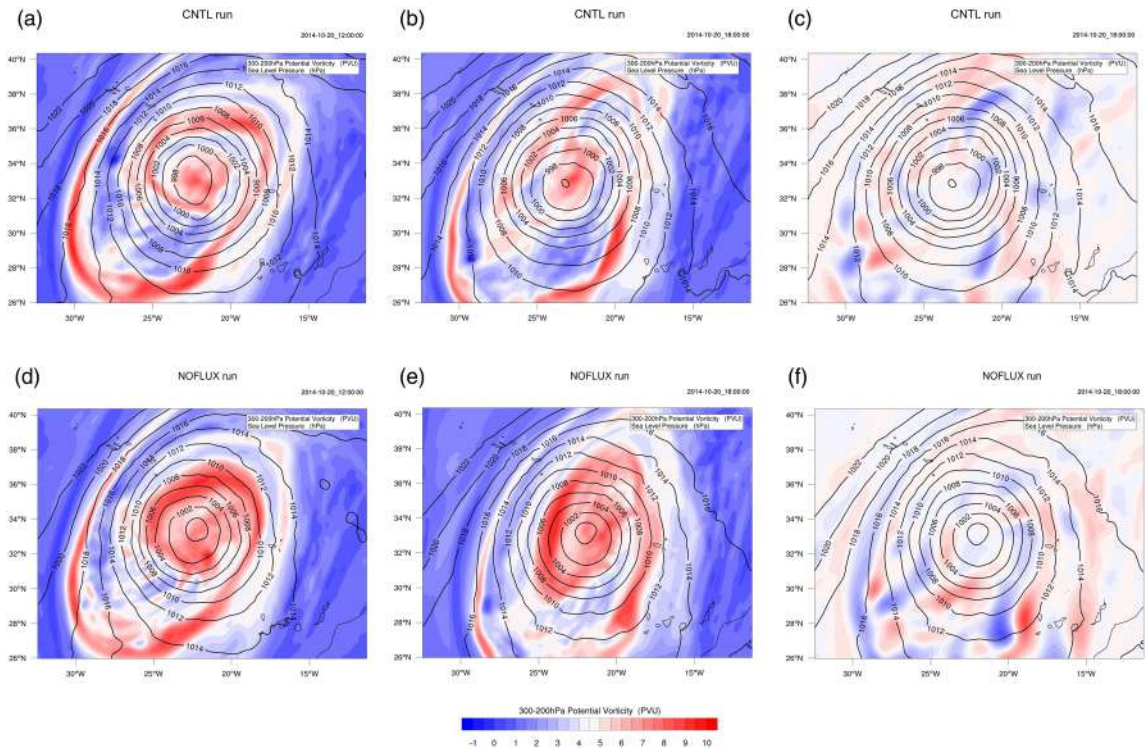

Figure 11. Same as Figure 10 except for 20 October 2014 at 1800 UTC.

heat is released. Furthermore, increase in the horizontal wind speed values and gradient at low levels, found in Figure 5 for the NOFLUX run, could contribute to the PV enhancement. There was again a general increase of the wind shear (Figures 12b and 12d). As with the other analyzed fields, there was a deviation of the cyclone center on the first day (Figure 12b). Furthermore, for the day on which there was no transition reproduced in the NOFLUX run, there was a noticeable constriction in the zone of smaller values around the cyclone center (purple zones in Figure 12c vs. those of Figure 12d). Moreover, because of the strong PV gradient near the cyclone center (Figures 11d and 11e), wind shear continued to be strong. These results could be one of the reasons why, in the NOFLUX run, there was no transition to a STC. Additionally, greater values of frontogenesis were obtained for the first day (Figure 8b), which enhanced rainfall (Figure 9b) and gave the cyclone a stronger frontal character. As in the analysis of Miglietta and Rotunno (2019), intense convection was inhibited upon the elimination of surface fluxes. This could explain the role of baroclinic instability in limiting system intensification and giving it an extratropical character.

In summary, in the CNTL run, PV values relaxed (Figures 10a–10c and 11a–11c). Analyzing the precipitation field, we found a substantial increase in convective precipitation (not shown), verifying the crucial role of convective processes during STC intensification. When surface turbulent heat fluxes were considered, transition into a STC was found (Figure 2), suggesting that atmospheric dynamic did not have much influence in this case. Therefore, a balance is needed in which surface fluxes intervene dynamically and thermodynamically to promote the transition into a STC. In contrast, in the NOFLUX run there was a more intense trough, characterized by a PV increase (Figures 10d–10f and 11d–11f). This PV enhancement boosted values of frontogenesis (Figures 8b and 8d) that in turn increased rainfall (Figures 9b and 9d). Wind increase was found around the northwest flank of the cyclone in conjunction with a frontal distribution of rainfall. No transition was found in this case, confirming the frontal nature of the system in the absence of surface fluxes.

3.3. Low-Level Winds During System Intensification

Regarding the importance of low-level winds for the intensification of the cyclone, WRF simulated 700- to 800-hPa wind speed and cloud top temperature (CTT) fields are analyzed in this subsection with the

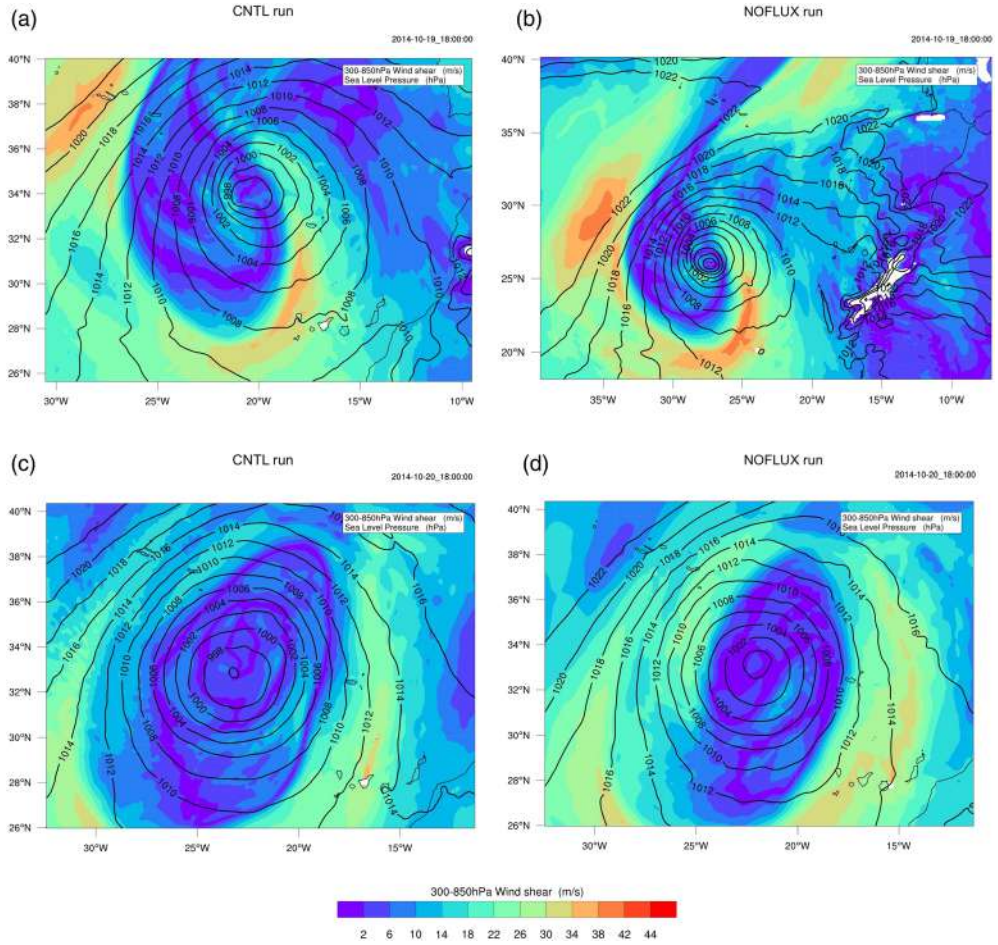

Figure 12. Same as Figure 3 except for 300- to 850-hPa wind shear (shaded, m/s) and sea level pressure (black contours, hPa).

CNTL and NOFLUX runs (Figure 13). Due to the importance of the low-level winds in the northwestern side of the cyclone for its intensification, an analysis around that area is going to be carried out in this subsection.

During the pre-STC period and in the CNTL run (Figure 13a), it is remarkable the similarity of the CTT structure (shaded in Figure 13a) with the satellite image of Figure 4, where a Shapiro-Keyser structure is noticed. Focusing on the northwestern side of the cyclone, wind barbs have a noticeable north-northeasterly direction. Regarding the wind speed values in that area, there is a predominance of values exceeding 24 km/hr at 700–800 hPa (Figure 13a). In the STC stage (Figure 13c), the CTT structure is again consistent with the observed in Figure 4, corroborating the WRF model simulation skillfulness. Furthermore, it is noticeable an increase in the wind speed values in that same area surpassing 33 km/hr at 700–800 hPa (Figure 13c).

In the NOFLUX run and during the pre-STC stage (Figure 13b), there was a remarkable slowing of wind speed. Regarding the northwestern area of the cyclone, we also found a north-northeasterly direction of the wind barbs and a reduction of wind speed contrary to the case in which the surface fluxes were considered (Figure 13a). Occurred also a prominent decrease in CTT (shaded in Figure 13b), corroborating the inhibition of intense convection by the lack of surface heat flux. During the STC stage (Figure 13d), there was a general increase in wind speed, especially in the analyzed area. Furthermore, there was a considerable reduction of CTT around the cyclone vortex (shaded values in Figure 13d). This confirms once more that in the absence of surface fluxes, cumulus convection and therefore cyclone intensification are limited (Miglietta & Rotunno, 2019).

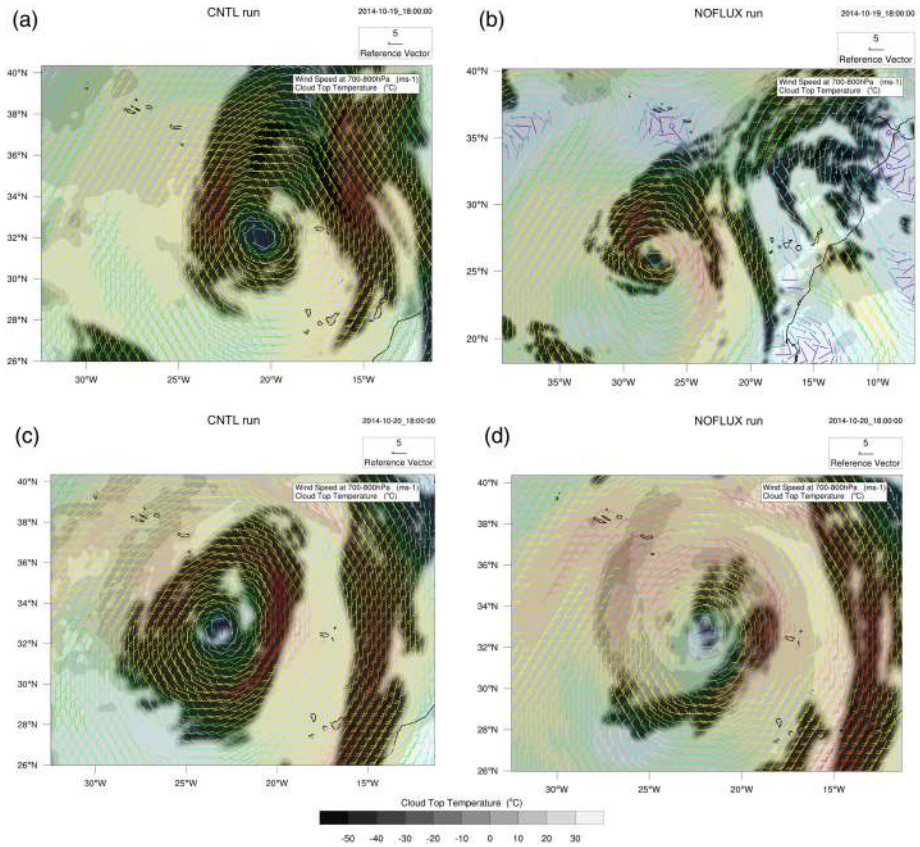

Figure 13. Same as Figure 3 except for wind speed at 700–800 hPa (barbs, m/s) and cloud top temperature (CTT) (shaded, °C).

Given the scarcity of observations over the oceans and the difficulty of obtaining reliable measurements near an intense storm with the characteristics of that studied here, so-called atmospheric motion vectors (AMVs) are very useful for characterizing cyclone development and intensification. Furthermore, several studies (Bedka & Mecikalski, 2005; Cordoba et al., 2016; García-Pereda & Borde, 2014) have found the use of AMVs advantageous in several weather analyses, owing to their wide coverage of large oceanic areas. AMVs are also considered important observational data for data assimilation systems in numerical weather prediction. According to several previous studies (Cardinali, 2009; Joo et al., 2012), the incorporation of AMVs via data assimilation has positive impacts on the predictive capability of operational numerical weather prediction systems.

We assessed the AMVs for the October 2014 STC. These vectors can be derived considering as many as seven MSG/SEVIRI satellite channel data (HRVIS, VIS06, VIS08, IR108, IR120, WV62, and WV73) and three GOES-N channel data (VIS07, IR107, and WV65). They are determined from the movement of cloud features and a cloud-height estimation algorithm based on visible, infrared, and water vapor satellite images, thereby providing wind speed and direction information. Two products are obtained, considering the pressure level (MACARO) and wind speed (MACAROSPEED).

In our work, MACARO and MACAROSPEED were obtained for the 2 days of our study, that is, 19 and 20 October at 1800 UTC (Figure 14). In order to contrast WRF simulations with observational data such as the AMVs, a comparison in the same previously analyzed northwestern area is assessed. Consequently, a red rectangle delimiting that area is depicted in Figure 14 due to the difference between displayed domains. From the AMV results for the pre-STC period in the selected area (Figures 14a and 14b), there are notable north-northeasterly low-level winds (bluish wind barbs at the left of Figure 14a) corresponding to the MACARO 700- to 800- and 800- to 900-hPa levels. These winds are consistent with the ones obtained for the WRF simulation (Figure 13a), confirming again the ability of the WRF model

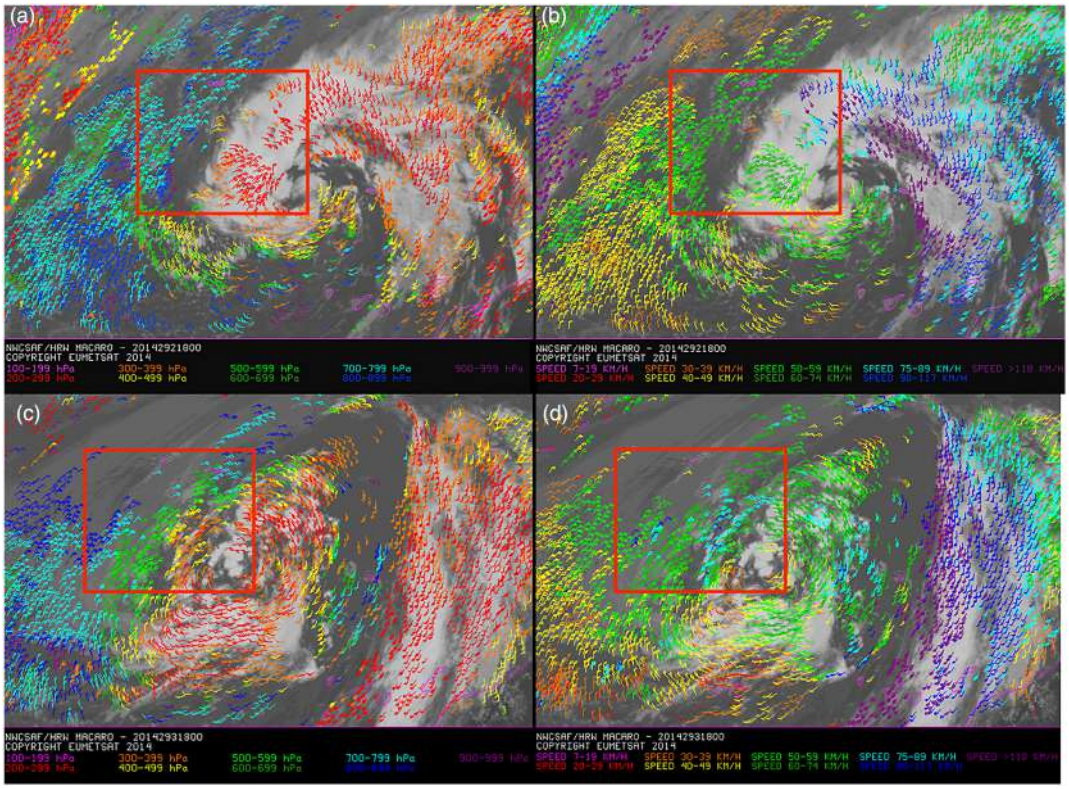

Figure 14. Atmospheric motion vectors on (top row) 19 and (bottom row) 20 October 2014 at 1800 UTC for (a, c) MACARO and (b, d) MACAROSPEED products. Source: EUMETSAT NWC SAF (AEMET).

for wind direction simulations. Because no low-level wind values could be obtained because of cloud thickness, high-level winds around the cyclone center (red barbs at bottom and right of red rectangle of Figure 14a) were analyzed. The red wind barbs again show a remarkable north-northeasterly direction. Some 300- to 500-hPa (yellow and orange wind barbs) and 500- to 600-hPa (greenish barbs) barbs show the same direction. These results corroborate the vertical wind structure on this day, which later promoted a symmetric cloudiness pattern with consequent cyclone intensification. In the same area of Figure 14b corresponding to the MACAROSPEED product, there was a preponderance of wind barbs exceeding 50 km/hr at the same levels of the MACARO product (Figure 14a), corroborating an underestimation from WRF results. Furthermore, wind speeds surpassing 50 km/hr were evident at lower (bluish wind barbs of Figure 14a) and upper (red wind barbs in rectangle of Figure 14a) levels. The strongest speeds were north of the cyclone (purple wind barbs at upper right of the selected area in Figure 14b), with a southeasterly direction and values exceeding 118 km/hr.

Focusing on the same area for the STC stage (Figures 14c and 14d) in the MACARO product (Figure 14c), wind barbs for the analyzed pressure levels had a general north-northeasterly direction (center left side of red rectangle in Figure 14c), which again confirms the WRF model skill for wind direction simulations. From the results related to the MACAROSPEED product (Figure 14d) and considering wind barb equivalence with the pressure levels in Figure 14c, we see a notable prevalence of wind barbs in excess of 50 km/hr (greenish barbs in Figure 14d), along with a few wind barbs to the northwest of the STC exceeding 75 km/hr (bluish barbs in Figure 14d). These results, confirm again an underestimation from WRF results when wind speed values around 33 km/hr are simulated. However, the agreement of WRF simulated wind direction with satellite data should be highlighted. Moreover, it is noticeable the consistence of the CTT structure with the satellite images of Figures 4 and 14, confirming a Shapiro-Keyser structure during the pre-STC stage.

4. Summary and Conclusions

The present study described the evolution of an EC during its transition to a STC in October 2014 near the Canary Islands. During this transition, an extratropical precursor resulting from a meridional atmospheric circulation evolved following a Shapiro-Keyser structure. This structure was mainly characterized by a bent-back warm/occluded front and underwent a warm seclusion process. Additionally, we evaluated the substantial influence of surface turbulent heat fluxes during the STC development and intensification. To this end, two WRF simulations were run, considering the presence and absence of surface turbulent heat fluxes.

The main conclusions are summarized as follows.

1. The results of the numerical model reveal a warm seclusion process. There was remarkable consistency between their θ_e values during the warm seclusion process (considering the surface turbulent heat fluxes) and those from the ECMWF shown over the MSG 6.2WV channel.
2. There was weakening of the warm seclusion process in the NOFLUX run. This demonstrates that in these cases, the thermal contribution was not critical. Furthermore, there was an outstanding increase in PV, adding weight to the dynamic contribution. Consequently, an intense frontogenesis area was simulated around the northwestern flank of the cyclone, intensifying the precipitation and wind fields. In conjunction with the lack of transition, these results confirm the frontal nature of the case study in the NOFLUX run.
3. The role of surface turbulent heat fluxes in the development, intensification, and subsequent transition into STC of the cyclone is highlighted. Strong latent heat release during the STC genesis caused a redistribution of PV that weakened wind shear. This promoted the development of the cyclone and its subsequent transition into a STC. Moreover, there was a considerable increase in convective precipitation, which substantiates the importance of convective processes during system intensification.
4. The underestimation of simulated low-level winds relative to observational AMV values highlights the use of observational data for supporting numerical model outputs.

The results of the present study encourage us to continue with the analysis and forecasting of these types of systems. Accordingly, additional cases will be used to analyze various key mechanisms for the determination of the genesis, location, transition, and evolution of those systems. As the WRF model is a nonspectral nudging one, the use of high-resolution reanalysis, such as ERA5 should be considered in order to improve/adjust possible displacements of these atmospheric systems. Furthermore, considering the application of data assimilation techniques, the model simulations could be improved by incorporating observational data such as AMVs. Therefore, the use of this technique in forthcoming studies could achieve more accurate simulations and consequently more realistic predictions for this type of cyclone.

Acknowledgments
This work was partially supported by research projects PCIN-2014-013-C07-04, PCIN2016-080 (UE ERA-NET Plus NEWA Project), CGL2016-78702-C2-1-R, CGL2016-78702-C2-2-R, and CGL2016-81828-REDT and the ECMWF special projects (SPESMART and SPESVALE). The second author was funded through PhD Grant BES-2014-067905 by the Spanish Ministry of Science, Innovation and University, and cofunded by the European Social Fund. We would like to express our gratitude to the anonymous reviewers for their rigorous review and helpful suggestions which improved this manuscript. Authors also thank the ECMWF for providing the analysis database (available at https://apps.ecmwf.int/mars-catalogue/?stream=oper&expver=1&month=oct&year=2014&type=an&class=od) and the NWC SAF of AEMET for providing the AMV images (http://www.nwcsaf.org/). We would also like to thank the NCEP GFS for supplying the initial and boundary conditions (available at https://rda.ucar.edu/datasets/ds083.2/index.html?hash=sfol-wl-/data/ds083.2#sfol-wl-/data/ds083.2?g=22014). The postprocessing software used for plotting the WRF model data has been the NCAR Command Language (NCL) software Version 6.4.0, and it is available at https://www.ncl.ucar.edu/index.shtml website. Regarding the data used to support the main conclusions of this work, they are mostly model outputs. The WRF model configuration scripts and postprocessing scripts are available at the following repository (DOI: https://doi.org/10.17632/t83g8jj4mb.1). Because this work is part of an ongoing research, the facilitated data set will be under embargo until 1 year from publication.

References

Bedka, K. M., & Mecikalski, J. R. (2005). Application of satellite-derived atmospheric motion vectors for estimating mesoscale flows. *Journal of Applied Meteorology*, *44*(11), 1761–1772. https://doi.org/10.1175/jam2264.1

Bentley, A. M., & Metz, N. D. (2016). Tropical transition of an unnamed, high-latitude, tropical cyclone over the eastern North Pacific. *Monthly Weather Review*, *144*, 713–736. https://doi.org/10.1175/MWR-D-15-0213.1

Browning, S. A., & Goodwin, I. D. (2013). Large-scale influences on the evolution of winter subtropical maritime cyclones affecting Australia's East Coast. *Monthly Weather Review*, *141*, 2416–2431. https://doi.org/10.1175/MWR-D-12-00312.1

Cardinali, C. (2009). Monitoring the observation impact on the short-range forecast. *Quaterly Journal of the Royal Meteorological Society*, *135*, 239–250.

Cavicchia, L., Pepler, A., Dowdy, A., & Walsh, K. (2019). A physically based climatology of the occurrence and intensification of Australian East Coast lows. *Journal of Climate*, *32*, 2823–2841. https://doi.org/10.1175/JCLI-D-18-0549.1

Cordeira, J. M., & Bosart, L. F. (2010). The antecedent large-scale conditions of the "Perfect Storms" of late October and early November 1991. *Monthly Weather Review*, *138*(7), 2546–2569. https://doi.org/10.1175/2010MWR3280.1

Cordeira, J. M., & Bosart, L. F. (2011). Cyclone interactions and evolutions during the "Perfect Storms" of late October and early November 1991. *Monthly Weather Review*, *139*, 1683–1707. https://doi.org/10.1175/2010MWR3537.1

Cordoba, M., Dance, S. L., Kelly, G. A., Nichols, N. K., & Waller, J. A. (2016). Diagnosing atmospheric motion vector observation errors for an operational high-resolution data assimilation system. *Quarterly Journal of the Royal Meteorological Society*, *143*(702), 333–341. https://doi.org/10.1002/qj.2925

Davis, C. A., & Bosart, L. F. (2003). Baroclinically induced tropical cyclogenesis. *Monthly Weather Review*, *131*, 2730–2747.

Davis, C. A., & Bosart, L. F. (2004). The TT problem: Forecasting the tropical transition of cyclones. *Bulletin of the American Meteorological Society*, *85*, 1657–1662.

Davolio, S., Miglietta, M. M., Moscatello, A., Pacifico, F., Buzzi, A., & Rotunno, R. (2009). Numerical forecast and analysis of a tropical-like cyclone in the Ionian Sea. *Natural Hazards And Earth Systems Sciences*, *9*, 551–562. https://doi.org/10.5194/nhess-9-551-2009

Dias Pinto, J. R., Reboita, M. S., & da Rocha, R. P. (2013). Synoptic and dynamical analysis of subtropical cyclone Anita (2010) and its potential for tropical transition over the South Atlantic Ocean. *Journal of Geophysical Research: Atmospheres*, *118*, 10,870–10,883. https://doi.org/10.1002/jgrd.50830

ECMWF, 2014: IFS Documentation, CY40R1 (consulted in https://www.ecmwf.int/en/publications/search/?solrsort=sort_label%20asc&secondary_title=%22IFS%20Documentation%20CY40R1%22).

Emanuel, K. A. (1986). An air–sea interaction theory for tropical cyclones. Part I: Steady-state maintenance. *Journal of the Atmospheric Sciences*, *43*, 585–605. https://doi.org/10.1175/1520-0469(1986)043<0585:AASITF>2.0.CO;2

Evans, J. L., & Braun, A. (2012). A climatology of subtropical cyclones in the South Atlantic. *Journal of Climate*, *25*, 7328–7340. https://doi.org/10.1175/JCLI-D-11-00212.1

Evans, J. L., & Guishard, M. P. (2009). Atlantic subtropical storms. Part I: Diagnostic criteria and composite analysis. *Monthly Weather Review*, *137*, 2065–2080. https://doi.org/10.1175/2009MWR2468.1

Galarneau, T. J., McTaggart-Cowan, R., Bosart, L. F., & Davis, C. A. (2015). Development of North Atlantic tropical disturbances near upper-level potential vorticity streamers. *Journal of the Atmospheric Sciences*, *72*(2), 572–597. https://doi.org/10.1175/JAS-D-14-0106.1

García-Pereda, J., & Borde, R. (2014). The impact of the tracer size and the temporal gap between images in the extraction of atmospheric motion vectors. *Journal of Atmospheric and Oceanic Technology*, *31*(8), 1761–1770. https://doi.org/10.1175/JTECH-D-13-00235.1

González-Alemán, J. J., Gaertner, M. A., Sánchez, E., & Romera, R. (2018). Subtropical cyclones near-term projections from an ensemble of regional climate models over the northeastern Atlantic basin. *International Journal of Climatology*, *38*, 454–465. https://doi.org/10.1002/joc.5383

González-Alemán, J. J., Valero, F., Martín-León, F., & Evans, J. L. (2015). Classification and synoptic analysis of subtropical cyclones within the northeastern Atlantic Ocean. *Journal of Climate*, *28*, 3331–3352. https://doi.org/10.1175/JCLI-D-14-00276.1

Gozzo, L. F., & da Rocha, R. P. (2013). Air-sea interaction processes influencing the development of a Shapiro-Keyser type cyclone over the subtropical South Atlantic Ocean. *Pure and Applied Geophysics*, *170*(5), 917–934. https://doi.org/10.1007/s00024-012-0584-3

Gozzo, L. F., da Rocha, R. P., Gimeno, L., & Drumond, A. (2017). Climatology and numerical case study of moisture sources associated with subtropical cyclogenesis over the southwestern Atlantic Ocean. *Journal of Geophysical Research: Atmospheres*, *122*, 5636–5653. https://doi.org/10.1002/2016JD025764

Guishard, M. P., Evans, J. L., & Hart, R. E. (2009). Atlantic subtropical storms. Part II: Climatology. *Journal of Climate*, *22*, 3574–3594. https://doi.org/10.1175/2008JCLI2346.1

Guishard, M. P., Nelson, E. A., Evans, J. L., Hart, R. E., & O'Connell, D. G. (2007). Bermuda subtropical storms. *Meteorology and Atmospheric Physics*, *97*(1-4), 239–253. https://doi.org/10.1007/s00703-006-0255-y

Hart, R. E. (2003). A cyclone phase space derived from thermal wind and thermal asymmetry. *Monthly Weather Review*, *131*(4), 585–616. https://doi.org/10.1175/1520-0493(2003)131<0585:ACPSDF>2.0.CO;2

Hulme, A. L., & Martin, J. E. (2009a). Synoptic- and frontal-scale influences on tropical transition events in the Atlantic basin. Part I: A six-case survey. *Monthly Weather Review*, *137*, 3605–3625. https://doi.org/10.1175/2009MWR2802.1

Hulme, A. L., & Martin, J. E. (2009b). Synoptic- and frontal-scale influences on tropical transition events in the Atlantic basin. Part II: Tropical transition of Hurricane Karen. *Monthly Weather Review*, *137*, 3626–3650. https://doi.org/10.1175/2009MWR2803.1

Joo, S., Eyre, J., & Marriott, R. (2012). The impact of metop and other satellite data within the Met Office global NWP system using an adjoint-based sensitivity method. *Monthly Weather Review*, *141*, 3331–3342. https://doi.org/10.1175/MWR-D-12-00232.1

Kuo, Y., Low-Nam, S., & Reed, R. J. (1991). Effects of surface energy fluxes during the early development and rapid intensification stages of seven explosive cyclones in the Western Atlantic. *Monthly Weather Review*, *119*, 457–476. https://doi.org/10.1175/1520-0493(1991)119<0457:EOSEFD>2.0.CO;2

Martin, J. E. (2006). *Mid-Latitude Atmospheric Dynamics: A First Course* (Vol. 324, pp. 33). Wiley,

Mazza, E., Ulbrich, U., & Klein, R. (2017). The tropical transition of the October 1996 Medicane in the Western Mediterranean Sea: A warm seclusion event. *Monthly Weather Review*, *145*, 2575–2595. https://doi.org/10.1175/MWR-D-16-0474.1

Miglietta, M. M., & Rotunno, R. (2019). Development mechanisms for Mediterranean tropical-like cyclones (Medicanes). *Quarterly Journal of the Royal Meteorological Society*, *145*(721), 1444–1460. https://doi.org/10.1002/qj.3503

Miller, D. K., & Katsaros, K. B. (1992). Satellite-derived Surface Latent Heat Fluxes in a Rapidly Intensifying Marine Cyclone. *Monthly Weather Review*, *120*, 1093–1107. https://doi.org/10.1175/1520-0493(1992)120<1093:SDSLHF>2.0.CO;2

Mills, G. A., Webb, R., Davidson, N. E., Kepert, J., Seed, A., & Abbs, D. (2010) The Pasha Bulker east coast low of 8 June 2007. CAWCR Technical Report, 023, 62 Pp. Centre for Australian Weather and Climate Research, Melbourne, Australia.

Posselt, D., & Martin, J. (2004). The effect of latent heat release on the evolution of a warm occluded thermal structure. *Monthly Weather Review*, *132*(2), 578–599. https://doi.org/10.1175/1520-0493(2004)132<0578:TEOLHR>2.0.CO;2

Powers, J. G., Klemp, J. B., Skamarock, W. C., Davis, C. A., Dudhia, J., Gill, D. O., et al. (2017). The Weather Research and Forecasting model: Overview, system efforts, and future directions. *Bulletin of the American Meteorological Society*, *98*(8), 1717–1737. https://doi.org/10.1175/BAMS-D-15-00308.1

Quitián-Hernández, L., Fernández-González, S., González-Alemán, J. J., Valero, F., & Martín, M. L. (2018). Analysis of sensitivity to different parameterization schemes for a subtropical cyclone. *Atmospheric Research*, *204*, 21–36. https://doi.org/10.1016/j.atmosres.2018.01.001

Quitián-Hernández, L., Martín, M. L., González-Alemán, J. J., Santos-Muñoz, D., & Valero, F. (2016). Identification of a subtropical cyclone in the proximity of the Canary Islands and its analysis by numerical modeling. *Atmospheric Research*, *178-179*, 125–137. https://doi.org/10.1016/j.atmosres.2016.03.008

Reed, R. J., Albright, M. D., Sammons, A. J., & Undén, P. (1988). The Role of Latent Heat Release in Explosive Cyclogenesis: Three Examples Based on ECMWF Operational Forecasts. *Weather and Forecasting*, *3*(3), 217–229. https://doi.org/10.1175/1520-0434(1988)0032.0.co;2

Schultz, D. M., Keyser, D., & Bosart, L. F. (1998). The effect of large-scale flow on low-level frontal structure and evolution in midlatitude cyclones. *Monthly Weather Review*, *126*, 1767–1791. https://doi.org/10.1175/1520-0493(1998)126<1767:TEOLSF>2.0.CO;2

Shapiro, M. A., & Keyser, D. (1990). In C. W. Newton, & E. Holopainen (Eds.), *Fronts, jets streams, and the tropopause. Extratropical Cyclones: The Erik Palmén Memorial Volume* (pp. 167–191). USA: American Meteorological Society.

Skamarock, W., & Klemp, J. (2008). A time-split nonhydrostatic atmospheric model for weather research and forecasting applications. *Journal of Computational Physics*, *227*(7), 3465–3485. https://doi.org/10.1016/j.jcp.2007.01.037

Yanase, W., Fu, G., Niino, H., & Kato, T. (2004). A Polar Low over the Japan Sea on 21 January 1997. Part II: A Numerical Study. *Monthly Weather Review*, *132*(7), 1552–1574. https://doi.org/10.1175/1520-0493(2004)1322.0.co;2